THE 4TH INTERNATIONAL CONFERENCE ON ALUMINUM ALLOYS

FATIGUE PROPERTIES OF AL 8090

H. Hargarter[1], G. Lütjering[1], J. Becker[2], and G. Fischer[2]
1. Technical University Hamburg-Harburg, 21071 Hamburg, Germany
2. Otto Fuchs Metallwerke, 58528 Meinerzhagen, Germany

Abstract

The fatigue crack growth behavior of Al 8090 was investigated in the critical short transverse direction of a rectangular forging with 80 mm thickness. The influence of four different environments was tested at stress ratios of 0.1 and 0.5: vacuum, laboratory air, and 3.5 % NaCl solutions with and without chromate inhibitors. In the aggressive environments the propagation rates were higher than in vacuum. In air and in the chloride solution with inhibitors fatigue crack propagation was strongly affected by crack closure although flat crack front geometries were found. The results were related to hydrogen embrittlement and to crack closure due to layers of reaction products on the fatigue fracture surface.

Introduction

The Aluminum-Lithium alloy 8090 was, besides of other applications, mainly intended as a replacement material for aerospace forgings, and good fatigue properties are therefore essential. The unique fatigue characteristics of Al-Li alloys have been the objective of many investigations, but still further insight into the mechanisms which control fatigue in Al 8090 has to be gained. Commonly, in heavy section forgings the short transverse (ST) direction is most critical. This seems to be especially true for Al 8090, since the material is susceptible to hydrogen embrittlement (1), and fracture toughness and ductility as well as the resistance against stress corrosion cracking have often been found to be the lowest in this direction (2).

This paper presents results of an investigation showing the effects of different environments and stress ratios on the fatigue crack growth behavior and fracture mode of Al 8090 loaded in ST-direction.

Experimental Procedure

The Al 8090 material was produced by Alcan, UK, as a conventional ingot casting, with a composition of Al-2.3Li-1.1Cu-0.8Mg-0.12Zr (wt.%). The material was forged at 480°C into a rectangular bar with dimensions of 80 x 140 x length [mm]. After forging, the material was homogenized for 2 hours at 530°C, water quenched, 3.3 % cold pressed and finally aged for 24 hours at 175°C, resulting in a slightly underaged condition (T 852).

The microstructure of the forging was investigated by light microscopy and transmission electron microscopy. The tensile properties were tested in ST- and L-direction on round specimens with a diameter of 5 mm and a gage length of 25 mm at an initial strain rate of 7×10^{-4} s^{-1}. The fracture toughness was evaluated on compact tension specimens (CT-specimens) with a thickness of 8 mm. The load was applied parallel to the ST-direction and the nominal crack propagation direction was parallel to the L-direction (ST-L orientation).

The fatigue crack propagation tests were performed with the same ST-L orientation and geometry of the CT-specimens. A servo-hydraulic closed-loop controlled testing machine was used, operating at a frequency of 30 Hz with a sinusoidal waveform. Crack propagation was monitored by a travelling light microscope. At selected crack velocities crack closure measurements were conducted at a reduced frequency of 0.1 Hz, using plots of load vs. crack opening displacement (COD) or back face strain (BFS).

Four different environments were used: vacuum ($\leq 10^{-6}$ Pa), ambient laboratory air, and two different aqueous solutions of NaCl at free corrosion potential: 3.5 wt.% NaCl (NaCl-pure) and 3.5 % NaCl + 0.3 % $NaCr_2O_7$ + 0.2 % Na_2CrO_4 (NaCl + inhibitor). The latter solution is often used in fatigue testing of other high strength Aluminum alloys. The tests were performed at room temperature (22°C) at stress ratios of R = 0.1 and 0.5.

Experimental Results

The microstructure of the alloy consisted mainly of the typical unrecrystallized pancake grains, which appeared fairly elongated in the L-direction (Fig. 1a). The grains had average dimensions of 50 x 100 x 1000 μm and contained low angle boundaries forming equiaxed subgrains with diameters of about 5 to 20 μm. In addition, large inclusions (Fe containing intermetallic particles) aligned in stringers in L-direction were found (Fig. 1b). The precipitate microstructure consisted mainly of coherent δ'-particles (Al_3Li) and semicoherent S'-plates, both homogeneously distributed throughout the matrix. Incoherent particles of the equilibrium phases were located along grain boundaries, leading to precipitate free zones.

The tensile properties are listed in Table 1. In the ST-direction especially the ductility was significantly lower than in the L-direction. In the ST-direction fracture occured mainly along large angle grain boundaries, which on a local scale adopted part of the shape of the equiaxed subgrains (Fig.2a). On the fracture surface sometimes "mats" of the Fe-containing inclusions were found, which contributed to the low ductility and the low fracture toughness (3). Higher magnifications revealed a ductile, dimpled type of fracture (Fig.2b).

The fatigue crack growth behavior in the different environments is shown in form of da/dN vs. ΔK-curves in Fig.3 for both stress ratios. In the aggressive environments, including laboratory air, fatigue crack propagation occurred at substantially lower ΔK-values than in vacuum. At a propagation rate of approximately 1 x 10^{-9} m/cycle the difference between the curves of R = 0.1 and R = 0.5 was much more pronounced in air than in vacuum. The lowest resistance to fatigue crack propagation was observed for the pure chloride solution. In this environment little difference in the propagation behavior between stress ratios of 0.1 and 0.5 was found, whereas in the NaCl-solution containing inhibitors a distinct difference was observed. With inhibitors, higher ΔK-values were necessary for crack propagation at R = 0.1 than at R = 0.5. Also it proved to be impossible at the lower stress ratio to establish slower propagation rates than approximately 1 x 10^{-8} m/cycle. This was in contrast to the tests in pure NaCl-solution in which stable fatigue crack propagation occurred with substantially slower propagation rates. It is believed that for NaCl-pure the fatigue behavior could be studied at slower crack velocities than actually tested in this investigation.

Typical plots of load vs. displacement or back face strain (which was used for tests in the aquaeous solutions) are compared in Fig.4. At a stress ratio of 0.1 some nonlinearity was observed in all the curves indicating crack closure effects. The crack closure effects in vacuum and NaCl-pure were negligibly small. In laboratory air and in the chloride solution with inhibitors significant crack closure effects were present (Fig. 4). At the stress ratio of 0.5 only in the NaCl + inhibitor-solution measurable crack closure was found.

Closure corrected ΔK-values (ΔK_{eff}) were calculated by using $P_{min,eff}$ as indicated in Fig. 4. The resulting "effective" da/dN-ΔK curves are shown in Fig. 5. Due to closure three fatigue crack propagation curves are shifted considerably (laboratory air tested at $R = 0.1$ and the two curves tested in NaCl + inhibitors). Also the effective stress ratios are included as data points for these three curves in Fig. 5 because crack closure not only affects ΔK but results also in an increase of the actual stress ratios. In air, the effective stress ratio increased from 0.1 to approximately 0.3, due to closure. For the solution of NaCl + inhibitors, effective stress ratios increased from 0.1 to about 0.4 and from 0.5 to about 0.6.

The crack front profiles were investigated on every specimen at selected crack velocities by sections perpendicular to the propagation direction. A very pronounced difference in roughness was found between vacuum and the other environments. In vacuum, at both stress ratios a rough crack front profile developed already at low ΔK-values, with only little change with rising ΔK (Fig. 6). No single portion of the profiles appeared to be oriented normal to the loading axis. In all other environments rather flat crack front profiles developed (Fig. 7-9), with no significant difference in surface roughness between the specimens tested at $R = 0.1$ and $R = 0.5$. Compared at equal crack velocities all aggressive environments resulted in the same profiles.

The fracture surfaces were also investigated and examples are shown in Figs. 10-13. Fig. 10 demonstrates the highly tortuous and facetted fracture surface of specimens tested in vacuum. The fracture mode clearly was crystallographic, as could also be concluded from the profiles of Fig.6. In air, a mixed fracture mode was observed. At high propagation rates the fracture surface was dominated by a slip band fracture mechanism. At intermediate propagation rates of approximately 1×10^{-8} m/cycle fracture occurred mainly along large angle grain boundaries (Fig. 11a). With decreasing propagation rates an increasing part of the fracture surface consisted of areas with transgranular fracture (Fig. 11b). In contrast to the facets formed in vacuum experiments, these areas were always orientated normal to the loading axis (see also Fig. 7a). In both NaCl-solutions crack propagation almost completely occurred as a brittle type of grain boundary fracture (Fig. 12 and 13). Some amount of transgranular fracture was observed at crack velocities below 1×10^{-8} m/cycle (Fig. 13b) and had a similar appearance like in air (Fig. 11b).

Discussion

Fatigue crack propagation is mainly controlled by the parameters: ductility, crack front geometrie, and crack closure (4). Also, it is well known that fatigue crack propagation is not only a function of the cyclic stress intensity, but also depends on the applied maximum stress intensity (K_{max}).

In vacuum any environmental effects are absent. Since only very little crack closure was found (Fig. 4) and since the crack front profiles were identical for both stress ratios (Fig. 6), crack closure cannot account for the difference between the curves tested at $R = 0.1$ and $R = 0.5$. At a given ΔK, the maximum stress intensity is much higher in case of the higher stress ratio and results in enhanced fatigue crack propagation rates. For both stress ratios a retarding contribution to fatigue crack propagation in vacuum can be deduced from the serrated crack front geometry observed.

The results of the tests in the other environments can be explained to a large extent on the basis of a hydrogen embrittlement mechanism. Hydrogen, introduced into the material by dislocation movement (5), leads to an embrittlement of the zone in front of the crack. This results in a lower fracture stress of material. Therefore, fatigue crack propagation becomes more dependent on the cyclic stress intensity, which controls the hydrogen transport, than on K_{max}. This behavior was found for the tests in pure chloride solution. In this environment the lowest

resistance against fatigue crack propagation was observed, and crack propagation depended only on ΔK.

The addition of chromate inhibitors should not affect hydrogen embrittlement, but the inhibitors hinder surface dissolution processes (6). The pronounced difference in fatigue crack propagation behavior between the tests in chloride solutions with and without inhibitors seems mainly to result from differences in crack closure (Fig. 5). In both solutions similar crack front geometries developed. Also, the rough surface observed in vacuum tests resulted in only little closure. Therefore, the high closure levels observed for the tests in NaCl + inhibitors might most likely be attributed to hydrides that remain on the fracture surface, whereas in pure chloride solution the hydrides can be dissolved. The presence of these hydrides as surface deposits could not be shown in this investigation because, unfortunately, the specimens were cleaned in an ultrasonic bath after testing to prevent further corrosion.

In air the pronounced closure effect seems also to result mainly from the fracture surface reaction products, since the crack front geometries were similar in air and the chloride solutions. The remaining difference after closure correction between the curves at low and high R-values indicate some influence of K_{max} (Fig. 5), similar to the behavior in vacuum.

Conclusions

The fatigue crack paths and propagation rates in Al 8090 - T 852 with ST-L orientation were strongly affected by the environment. Humid air and chloride solutions led to much enhanced crack growth rates as compared to vacuum. A hydrogen embrittlement mechanism appears most reasonable to explain the results. Pronounced closure effects were found in air and in the chloride solution with chromate inhibitors, suggesting a crack retardation mechanism mostly due to surface reaction products. In contrast to fatigue testing in vacuum, in which crystallographic fracture was predominant, crack propagation in aggressive environments occurred mainly along grain boundaries.

References

1. N.J.H. Holroyd et al., Aluminum-Lithium Alloys III, ed. C. Baker et al. (The Institute of Metals, London, 1986), p.310.

2. W.E. Quist, G.H. Narayanan, Aluminum Alloys - Contemporary Research and Applications, ed. A.K. Vasudevan and R.D. Doherty, Treatise on Materials Science and Technology, Vol. 31, (Academic Press Inc., 1989), p.219.

3. H. Hargarter, G. Lütjering, J. Becker and G. Fischer, 2nd Int. Conf. on Mechanical Alloying for Structural Applications, ed. J.J. deBarbadillo, F.H. Froes and R. Schwarz, (ASM International, Ohio, 1993), p.313.

4. G. Lütjering, A. Gysler and L. Wagner, Sixth World Conf. on Titanium, (les éditions de physique, Les Ulis Cedex, 1988), p.71.

5. J. K. Tien et al., Met. Trans. A, 7A (1976), p.821.

6. R. Braun, H. Buhl, 4th Aluminium-Lithium Conf., ed. G. Champier et al., (les éditons de physique, Les Ulis Cedex, 1987), p.C3-847.
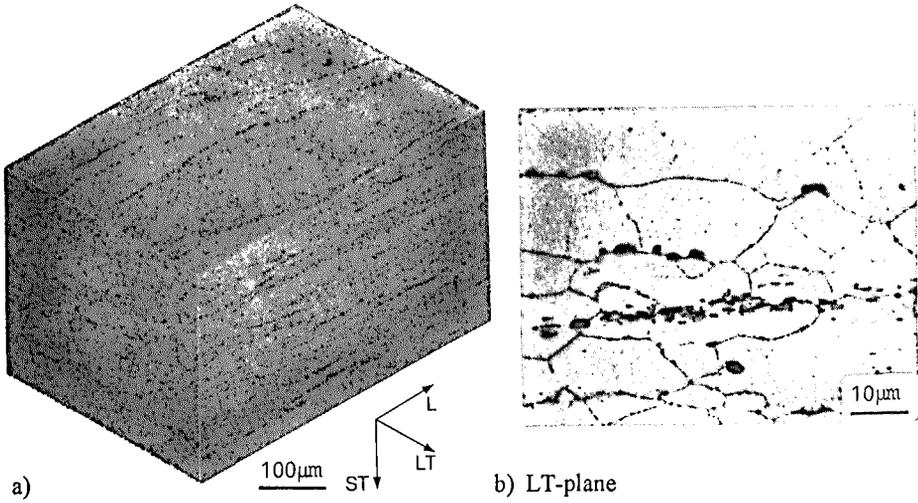
a)

b) LT-plane

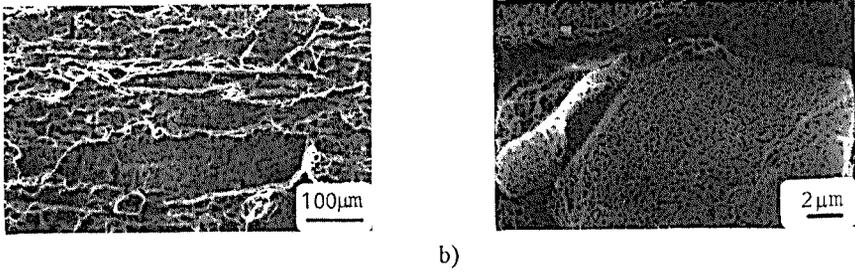Fig. 1 - Microstructure (LM)

a)

b)

Fig. 2 - Tensile fracture surface (SEM)

Table I. Mechanical properties

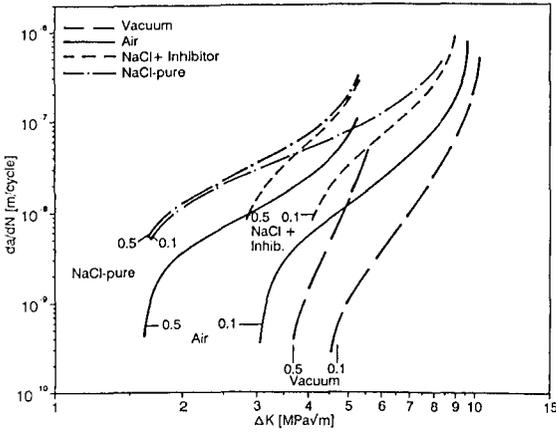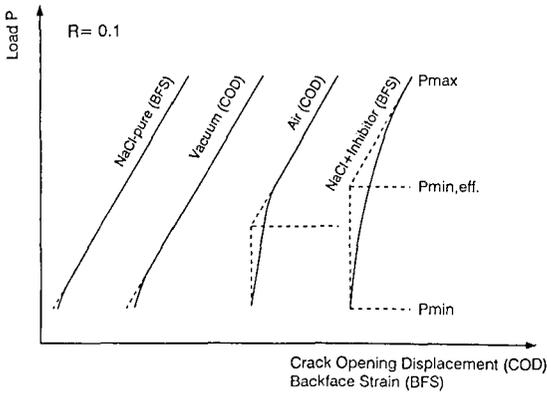|	$\sigma_{0.2}$ (MPa)	UTS (MPa)	σ_F (MPa)	TE (%)	ε_F	K_{Ic} [MPa m$^{1/2}$]
L	460	530	620	7.6	0.22	--
ST	385	515	535	3.9	0.04	11 (ST-L)

Fig. 3
Nominal da/dN-ΔK curves
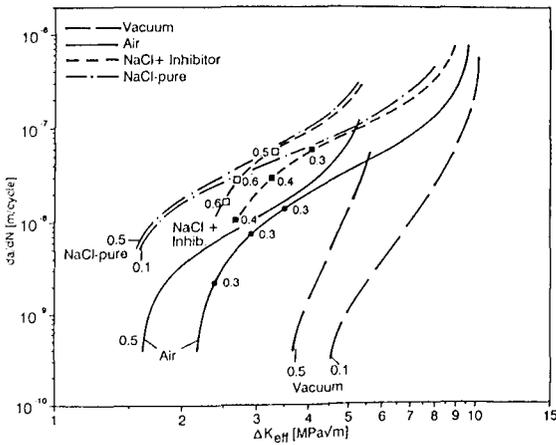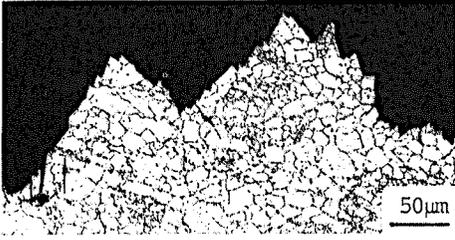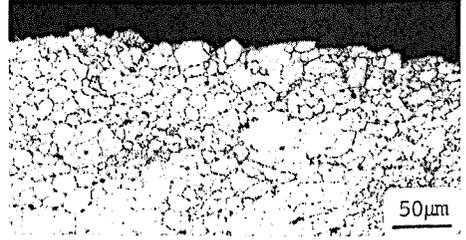for R = 0.1 and R = 0.5

Fig. 4
Typical COD-curves from
tests at R = 0.1

Fig. 5
Closure corrected da/dN-ΔK
curves. Data points indicate
the effective stress ratios

425
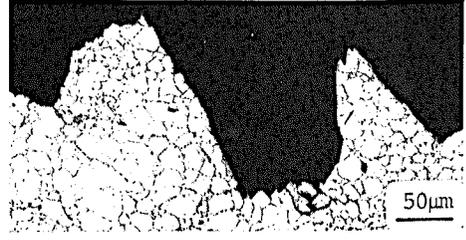
a) R = 0.1   b) R = 0.5
Fig. 6 - Crack profiles at da/dN = 1 x 10^{-8} m/cycle in vacuum
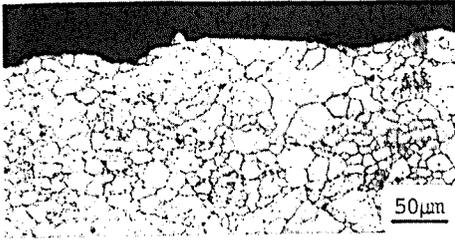
a) R = 0.1   b) R = 0.5
Fig. 7 - Crack profiles at da/dN = 1 x 10^{-8} m/cycle in air
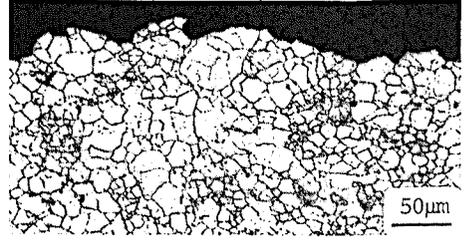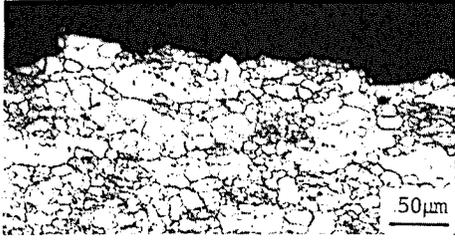
a) R = 0.1   b) R = 0.5
Fig. 8 - Crack profiles at da/dN = 1 x 10^{-8} m/cycle in NaCl + inhibitor solution
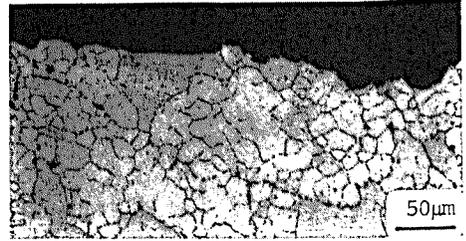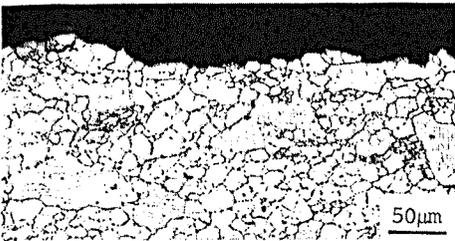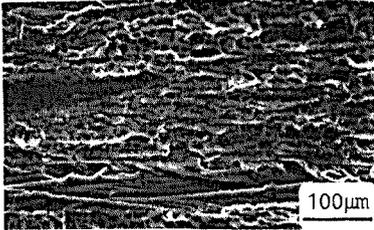

a) R = 0.1   b) R = 0.5
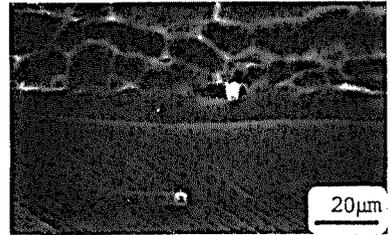Fig. 9 - Crack profiles at da/dN = 1 x 10^{-8} m/cycle in NaCl-pure solution
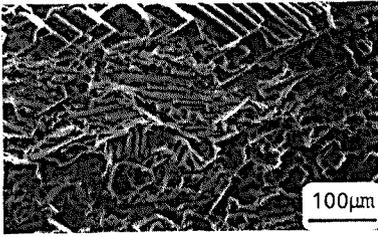
a) R = 0.1, da/dN = 1 x 10^{-8} m/cycle b) R = 0.1, da/dN = 1 x 10^{-9} m/cycle
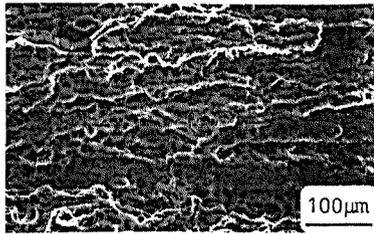Fig. 10 - Fatigue fracture surface (SEM), vacuum

a) R = 0.1, da/dN = 1 x 10^{-8} m/cycle b) R = 0.5, da/dN = 1 x 10^{-9} m/cycle
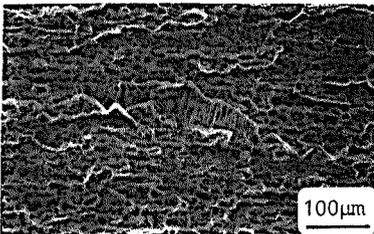Fig. 11 - Fatigue fracture surface (SEM), air

a) R = 0.1, da/dN = 5 x 10^{-8} m/cycle b) R = 0.1, da/dN = 5 x 10^{-8} m/cycle
Fig. 12 - Fatigue fracture surface (SEM), NaCl + inhibitor solution

a) R = 0.1, da/dN = 1 x 10^{-8} m/cycle b) R = 0.1, da/dN = 1 x 10^{-8} m/cycle
Fig. 13 - Fatigue fracture surface (SEM), NaCl-pure solution

427